University of Arizona
Tucson Arizona 85721

LEADING-EDGE RECEPTIVITY FOR BLUNT-NOSE BODIES

NASA Grant NAG-1-1135
Semi-Annual Progress Report

P.W. Hammerton and E.J. Kerschen

July 1992

This research program investigates boundary-layer receptivity in the leading edge region for bodies with blunt leading edges. Receptivity theory provides the link between the unsteady disturbance environment in the freestream and the initial amplitudes of instability waves in the boundary layer. This is a critical problem which must be addressed in order to develop more accurate prediction methods for boundary-layer transition.

Previous analyses of leading-edge receptivity have been restricted to the case of a zero-thickness flat plate in symmetric flow at low Mach number. Singular perturbation techniques were utilized, based on a large Reynolds number for the unsteady motion ($\epsilon = (\omega\nu/U_\infty^2)^{1/6} \ll 1$). In this project we are extending the theory to include the effect of a parabolic leading edge, and also the effect of aerodynamic loading. The influence of nose bluntness enters through the parameter $S = \omega r_n/U_\infty$, where r_n is the nose radius of the parabola. Our theory assumes that $S = O(1)$.

Results for a symmetric base flow with a parallel acoustic disturbance are discussed in Ref. 1. Only the salient points are reproduced here. The boundary layer structure is illustrated in Fig. 1. Parabolic coordinates ξ, η are used throughout. The streamwise and transverse coordinates ξ and η have been nondimensionalized by the convective wavelength, U_∞/ω, and by $\epsilon^3 U_\infty/\omega$, respectively. Unlike the flat-plate case, the mean boundary layer equation must be solved numerically. This was accomplished using a Keller Box method. The solution must then be matched to the large ξ asymptotic limit,

$$\Psi = \xi\left(F(\eta) + 2A_1 g(\eta)\frac{\log w}{w^2} + (B_1 g + f(\eta))\frac{1}{w^2} + O(w^{-3.774})\right), \qquad w = \frac{\xi}{S^{1/2}}. \tag{1}$$

Here $F(\eta)$ is the Blasius (flat-plate) solution, $g = \eta F' - F$ and f is the solution of a third-order ODE. The numerical constant A_1 is determined by the condition that vorticity decays exponentially away from the body, but B_1 can only be determined by comparison to the numerical solution. The extraction of B_1 is illustrated in Fig. 2.

Far downstream ($\xi \gg 1$), the unsteady disturbance in the boundary layer is of the form

$$\psi \sim \bar{\psi}(\eta, \xi, S) + \sum_{i=1} C_i(S)\psi_i(\eta, \xi, S). \tag{2}$$

The functions $\bar{\psi}$, ψ_i are determined by the *local properties* of the geometry and the freestream disturbance in the far-downstream region. For an acoustic freestream disturbance, $\bar{\psi}$ corresponds to a Stokes shear wave. The asymptotic eigensolutions ψ_i depend only on the downstream geometry and are independent of the freestream disturbance. However, the coefficients C_i are determined by the

receptivity process which occurs in the region $\xi = O(1)$. Specifically, the first asymptotic eigensolution ψ_1 matches onto the Tollmien-Schlichting wave which becomes unstable farther downstream in the boundary layer. Thus it is through $C_1(S)$ that the freestream disturbance determines the magnitude of the unstable disturbance, and hence C_1 is called the receptivity coefficient.

The asymptotic eigensolutions ψ_i decay exponentially with downstream distance and they are also inverse ordered, i.e., the ratio ψ_i/ψ_{i+1} becomes exponentially small for $\xi \gg 1$. Thus, it is difficult to obtain C_1 from a direct numerical solution of the Linearised Unsteady Boundary Layer Equation (LUBLE). This problem is circumvented by extending the analysis and the numerical solution to the complex ξ plane and choosing $\arg(\xi)$ such that ψ_1 grows exponentially. In this region of the complex plane the asymptotic eigensolutions assume a normal ordering, with ψ_1 dominating both $\bar{\psi}$ and the higher terms in the above series. The Receptivity Coefficient $C_1(S)$ can then be obtained by comparing the numerical results with the asymptotic form of ψ_1. Essentially, the known analytical form of the asymptotic eigensolution is utilized to extrapolate the numerical results to $\xi \to \infty$. For $\xi \gg 1$, the first asymptotic eigensolution has the form

$$\psi_1 \sim (1 + b_1\xi^{-0.774} + b_2\xi^{-1}\log^2\xi + b_3\xi^{-1}\log\xi + b_4\xi^{-1} + \ldots)\xi^{\tau}p(\eta)e^{T(\xi)} \tag{3}$$

where

$$T(\xi) = -\frac{\lambda\xi^3}{U_0'}\left\{\tfrac{1}{3} - 2A_1\frac{\log w}{w^2} + (2A_1 + \tfrac{3}{2} - B_1)\frac{1}{w^2}\right\}. \tag{3a}$$

The fact that there are several terms in (3) which are similar in magnitude makes the extrapolation difficult, and numerical integration must be continued up to very large values of ξ to obtain accurate estimates of the Receptivity Coefficient C_1.

The variation of C_1 with S for an acoustic disturbance parallel to the body axis was given in Ref. 1. A dramatic decrease in receptivity with increasing nose radius was reported. At $S = 0.3$ the Receptivity Coefficient C_1 drops to 10% of that for a flat plate. The conclusion to be drawn is that a favorable pressure gradient not only shifts the point of neutral stability further downstream, but also inhibits the receptivity process. An asymptotic theory for small S has now been completed. In this case the region close to the nose is quasi-steady and in the region $\xi = O(1)$, which dominates the receptivity process, the body surface approaches a flat plate. This analysis predicts an *increase* in receptivity for small S,

$$|C_1(S)| \sim |C_1(0)|(1 + 3.13S). \tag{4}$$

Comparison with numerical results (Fig. 3) shows that this is indeed true, but also reveals that the $S \ll 1$ theory is useful only for very small S and that the maximum increase in $|C_1|$ is only of the order of 3%. The reason behind this increase is not fully understood. However, for all practical purposes this very local increase can be ignored.

The Receptivity Coefficient has also been calculated for different types of freestream disturbances. In carrying out these calculations we take advantage of the fact that the evolution of the unsteady disturbance (2) with downstream distance in the complex ξ plane occurs in two distinct

stages. During the first stage the unsteady disturbance becomes dominated by the single term $C_1(S)\psi_1(\eta,\xi,S)$, which grows exponentially relative to the other terms in (2). Due to the exponential dependence only moderately large values of ξ are necessary for this first stage to be completed. The second stage corresponds to the evolution of the function ψ_1 according to the asymptotic form (3). The higher-order terms in (3a) are algebraic and therefore become unimportant only for much larger values of ξ. In extracting the Receptivity Coefficient for an acoustic disturbance parallel to the body axis, it was necessary to continue the numerical computation out to distances where (3) is dominated by the first few terms. However, since this computation provides information regarding the evolution of ψ_1, in the computations for other types of freestream disturbances it is only necessary to extend the computations to the point where the first stage has been completed.

For an incoming acoustic disturbance at angle θ to the axis of symmetry, the Receptivity Coefficient is given by

$$C_1(S) = \cos\theta C_a(S) + a^{1/2}\sin\theta C_b(S) \tag{5}$$

where a is the airfoil half-chord, non-dimensionalized by the convective wavelength. This is valid for $a \gg \epsilon^{-2}$, ensuring that transition occurs towards the leading edge. The magnitudes and arguments of C_a and C_b are plotted in Figs. 4 and 5. It is seen that the receptivity due to the asymmetric component of the disturbance is much larger than that due to the symmetric component, but it also reduces faster with S than the symmetric component. This is illustrated more clearly in Figures 6 and 7, where the total receptivity is illustrated for a realistic non-dimensional chord length, $a = 225$. In Fig. 6 the variation $|C_1|$ with incidence angle is illustrated for various values of nose radius. In Fig. 7 the modulus of the receptivity is plotted against S for various acoustic incidence angles. For small values of S, receptivity levels rise rapidly with increasing angle of incidence of the acoustic wave. However at larger values of S, this increase is less marked. These results are for an airfoil with no induced circulation due to the oblique disturbance. For a body with sharp trailing edge, an additional contribution to the slip velocity due to enforcement of the unsteady Kutta condition must be included. This will be calculated in the near future.

Work is now proceeding to determine the receptivity due to a convected vorticity gust. In contrast to the flat-plate case, the vorticity is distorted by gradients in the inviscid flow field near the leading edge. The slip velocity on the body due to the gust is obtained using Rapid Distortion Theory.

We are also extending our theory to incorporate the influence of mean aerodynamic loading on receptivity. This effect has been ignored in previous studies because loading is incompatible with the zero-thickness, flat-plate model. Aerodynamic loading produces an adverse pressure gradient on the upper surface, and we anticipate that this may lead to a substantial increase in the Receptivity Coefficient.

The asymptotic analysis of the steady and unsteady boundary layer flow in the nose region, for an airfoil at non-zero angle of attack has now been completed. This will be published in detail elsewhere. Here we give a few of the more important results. For an angle of attack α, the steady

boundary layer solution well downstream of the nose is given by

$$\Psi \sim (\cos\alpha + \mu)\left(F + \frac{\mu p}{w} + \frac{2A_1 g \log w}{w^2} + \frac{(B_1 g + f)}{w^2} + \frac{2\mu q \log w}{w^2} + \frac{\mu r}{w^3} + O(w^{-3.774})\right), \qquad (6)$$

where $\mu = \sin\alpha(a/S)^{1/2}$ and $w = \cos\alpha\xi + \mu$, and f, g, p, q, r are functions of η given by a set of third-order ODEs. The stagnation point is given by $w = 0$.

As in the symmetric case, A_1 is determined by the condition of exponential decay of vorticity, but now depends on μ. $B_1(\mu)$ is determined by comparing numerical solutions to the asymptotic solution. This has been carried out and B_1 obtained for various values of μ. All the terms included in the expansion of Ψ are necessary in order to calculate the eigenfunction for the unsteady disturbance in the boundary layer. However, the need to include so many terms in the expansion naturally makes the analysis considerably more involved. Finally the asymptotic eigenfunction is found to be

$$\psi_1 \sim (1 + b_1\xi^{-0.774} + b_2\xi^{-1}\log^2\xi + b_3\xi^{-1}\log\xi + b_4\xi^{-1} + \ldots)\xi^r p(\eta) e^{T(\xi)} \qquad (7a)$$

where

$$T(\xi) = T_{\mu=0} - \mu\left[\frac{\lambda\xi^3}{U_0'}\left\{\frac{a}{w} + \frac{b\log w}{w^2} + \frac{c\log^2 w}{w^3} + \frac{d\log w}{w^3}\right\}\right] \qquad (7b)$$

and a, b, c, d are known functions of μ. The computer code used for the symmetric case is currently being modified to solve this modified LUBLE. The first results are expected to be available in the next month. For acoustic disturbances in the freestream, the coefficient of receptivity will now be a function of three parameters, angle of attack, nose radius and acoustic angle of incidence.

In summary, our research to date has determined the influence of nose radius on leading-edge receptivity for the case of symmetric flow past a parabolic leading edge. Results have been obtained for a variety of acoustic freestream disturbances, and calculations for the case of vortical freestream disturbances are presently being carried out. In addition, the asymptotic theory has been extended to include the influence of mean aerodynamic loading in the leading-edge region, and the related computer programs are presently being developed. This work will provide answers to fundamental questions concerning leading-edge receptivity, i.e., the influence of the airfoil nose radius and mean aerodynamic loading. These issues must be understood in order to apply receptivity theory to realistic geometries.

References

1. Hammerton, P.W., & Kerschen, E.J., "Effect of nose bluntness on leading-edge receptivity". Submitted to *Proceedings of Transition & Turbulence Workshop*, NASA LaRC, July 1991.

Figure Captions

Figure 1. A schematic illustration of the boundary layer structure for a parabolic body in a symmetric mean flow. The three decks in the Orr-Sommerfeld region are (i) the viscous wall layer; (ii) the main inviscid layer; and (iii) the outer irrotational layer.

Figure 2. Plot of $G(Z) = (\log Z)^{-1} Z([\phi'' - F'']/F'')_{\eta=0}$ against $(\log Z)^{-1}$, where $Z = w^2$. Comparison with the large w asymptotic form yields $B_1 \approx 2.08$.

Figure 3. Comparison of asymptotic and numerical results for very small S. Numerical results are marked with squares.

Figure 4. Variation of the amplitude of the Receptivity Coefficients as a function of Strouhal number, S. C_a and C_b are the Receptivity Coefficients for the symmetric and antisymmetric components of freestream disturbance respectively.

Figure 5. Variation of the phase of the Receptivity Coefficients as a function of Strouhal number, S.

Figure 6. Variation of $|C|$ with acoustic incidence angle θ, for non-dimensional airfoil chord length $a = 225$.

Figure 7. Variation of $|C|$ with S for various acoustic incidence angles, with the same airfoil chord length as Figure 6.

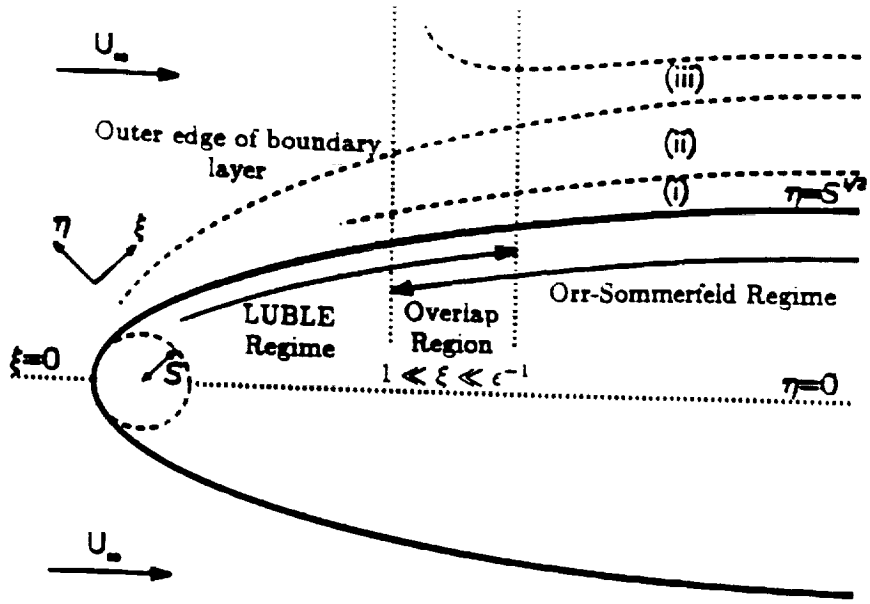

Figure 1. A schematic illustration of the boundary layer structure for a parabolic body in a symmetric mean flow. The three decks in the Orr-Sommerfeld region are (i) the viscous wall layer; (ii) the main inviscid layer; and (iii) the outer irrotational layer.

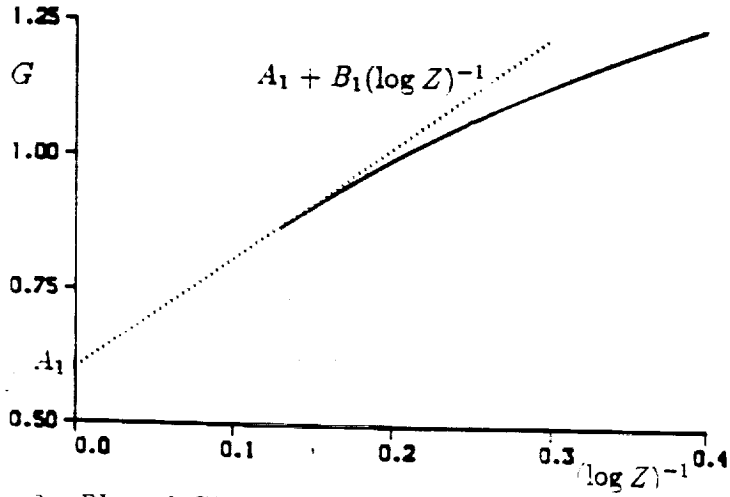

Figure 2. Plot of $G(Z) = (\log Z)^{-1} Z([\phi'' - F'']/F'')_{\eta=0}$ against $(\log Z)^{-1}$, where $Z = w^2$. Comparison with the large w asymptotic form yields $B_1 \approx 2.08$.

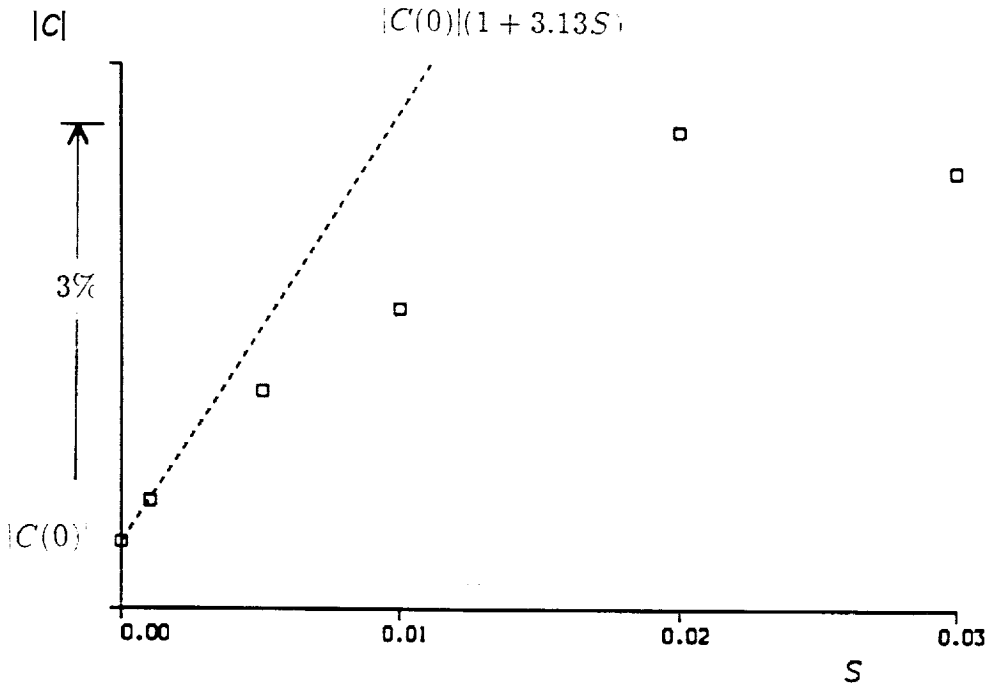

Figure 3. Comparison of asymptotic and numerical results for very small S. Numerical results are marked with squares.

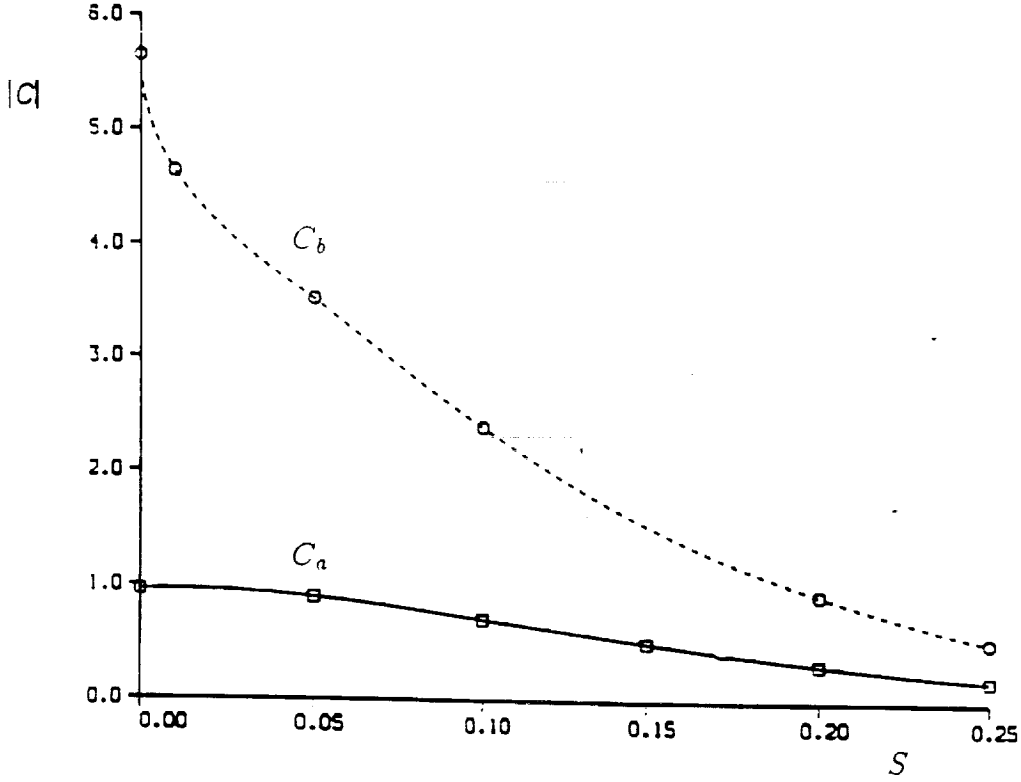

Figure 4. Variation of the amplitude of the Receptivity Coefficients as a function of Strouhal number, S. C_a and C_b are the Receptivity Coefficients for the symmetric and antisymmetric components of freestream disturbance respectively.

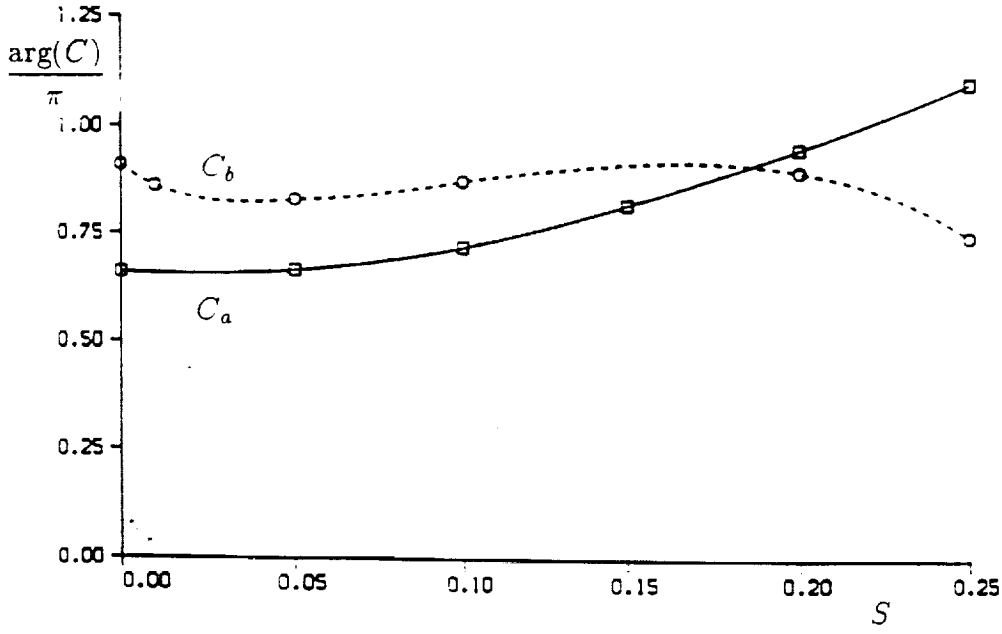

Figure 5. Variation of the phase of the Receptivity Coefficients as a function of Strouhal number, S.

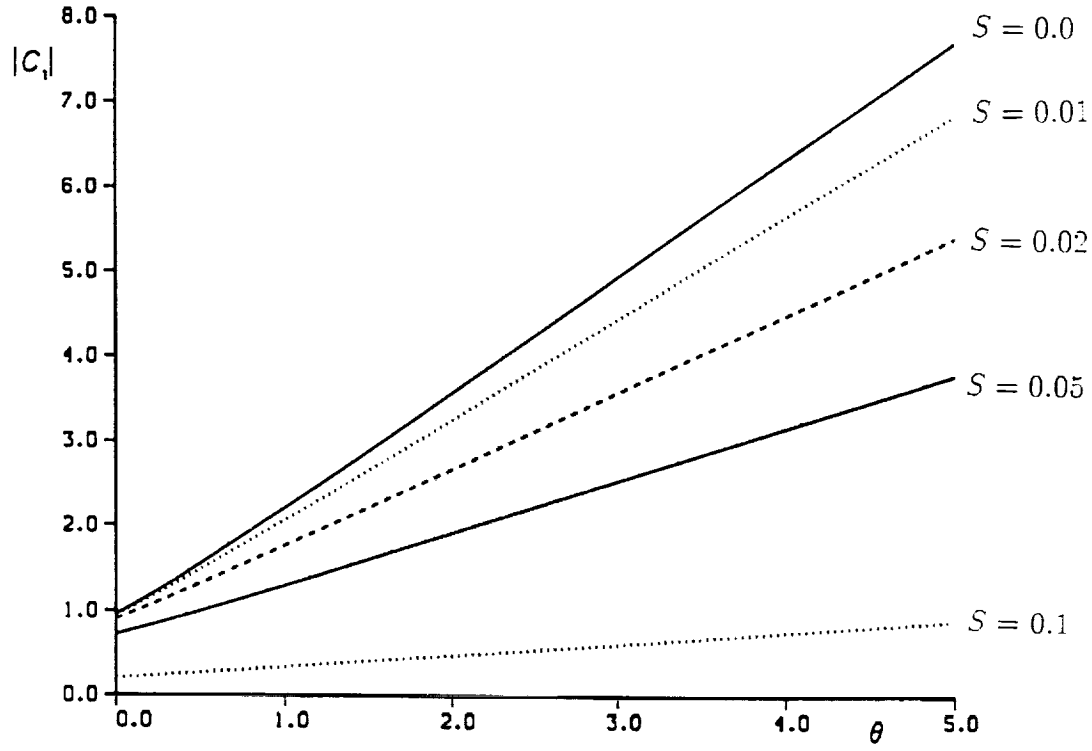

Figure 6. Variation of $|C|$ with acoustic incidence angle θ, for non-dimensional airfoil chord length $a = 225$.

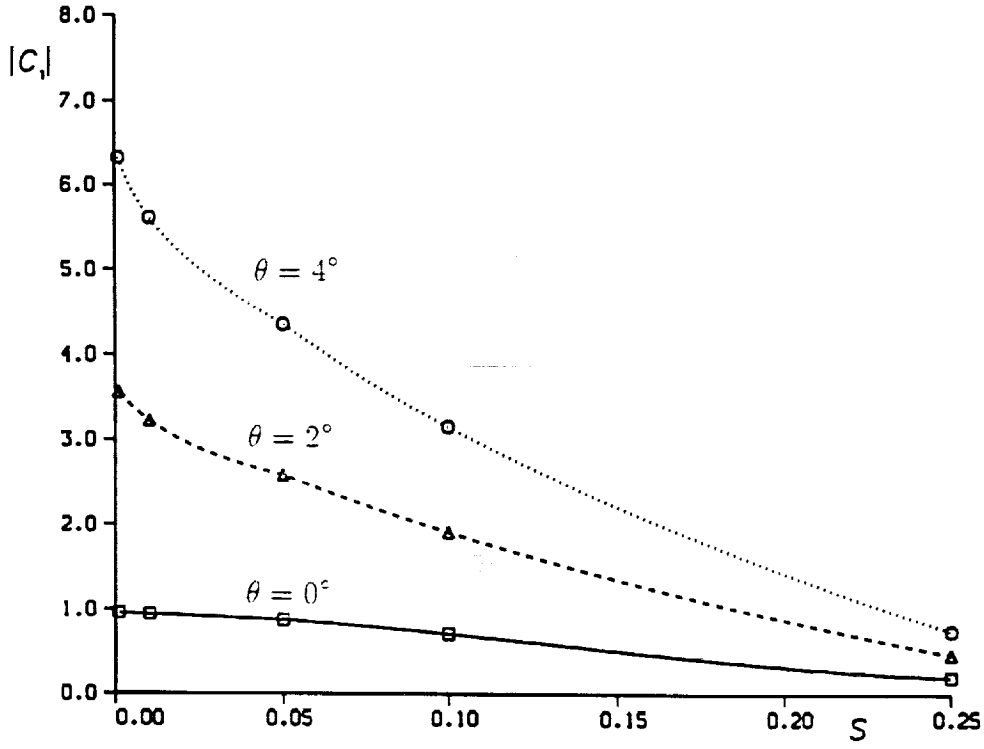

Figure 7. Variation of $|C|$ with S for various acoustic incidence angles, with the same airfoil chord length as Figure 6.